Atomistic Global Optimization X: A Python package for optimization of atomistic structures

Mads-Peter V. Christiansen,[1] Nikolaj Rønne,[1] and Bjørk Hammer[1, a)]
Center for Interstellar Catalysis, Department of Physics and Astronomy, Aarhus University, DK-8000 Aarhus, Denmark

Modelling and understanding properties of materials from first principles require knowledge of the underlying atomistic structure. This entails knowing the individual chemical identity and position of all atoms involved. Obtaining such information for macro-molecules, nano-particles, clusters, and for the surface, interface, and bulk phases of amorphous and solid materials represents a difficult high-dimensional global optimization problem. The rise of machine learning techniques in materials science has, however, led to many compelling developments that may speed up structure searches. The complexity of such new methods has prompted a need for an efficient way of assembling them into global optimization algorithms that can be experimented with. In this paper, we introduce the Atomistic Global Optimization X (AGOX) framework and code, as a customizable approach that enables efficient building and testing of global optimization algorithms. A modular way of expressing global optimization algorithms is described and modern programming practices are used to enable that modularity in the freely available AGOX python package. A number of examples of global optimization approaches are implemented and analyzed. This ranges from random search and basin-hopping to machine learning aided approaches with on-the-fly learnt surrogate energy landscapes. The methods are show-cased on problems ranging from supported clusters over surface reconstructions to large carbon clusters and metal-nitride clusters incorporated into graphene sheets.

I. INTRODUCTION

Global optimization is a prerequisite for the computational treatment of materials at the atomic level. The application of quantum mechanics to predict the properties of materials requires knowledge of the positions of all the atoms that make up the material. The positions that occur in reality will often be very close to those that minimize the total quantum mechanical energy, whereby the importance of global optimization for atomistic structure is evident. The problem may be visualized as finding the lowest valley in a high-dimensional landscape, the potential energy surface (PES). This surface may be described at different levels of theory, from crude distance-based pair-potentials to sophisticated calculations treating the particles at the quantum level. With increased accuracy comes increased computational cost, therefore global optimization methods that efficiently search the PES for the lowest energy minima are necessary. Computational approaches that utilize global optimization have received significant attention and led to impressive results.[1–5]

A multitude of optimization algorithms have been proposed from simulated annealing[6] through basin-hopping[7] and minima-hopping[8] methods to evolutionary algorithms[9–14] to ab-initio-random structure search[15] and particle swarm algorithms[16,17] to mention a few of the most successful methods. In recent years, machine learning has become a central topic in computational materials science. A prominent example of which is the ever increasing accuracy of machine learned potential energy surfaces, colloquially referred to simply as machine learn-

ing potentials.[18–33] Machine learning has also led to substantial improvements for simulation tasks in computational material science, such as machine learning potential based molecular-dynamics simulations for investigating properties of materials,[34–41] optimization algorithms exploiting machine learning potentials[42–62] or machine learning methods for guided exploration of the PES.[63–74]

With the speed of advancement in the materials science and machine learning communities it is essential that software tools are available that allow quick experimentation. This is especially true for global optimization (GO), an open-ended subject with room for new and improved algorithms. In GO, the aim is to identify the optimum solution for a complex target function. Being goal-driven, any GO method that does so is legitimate if the goal is eventually reached, and hence experimentation with the computational strategy is welcomed. This contrasts other tasks in materials science, such as solving the Kohn-Sham equations and calculating forces in density functional theory calculations, or propagating atomic positions in molecular dynamics simulations, where the methods are governed by well-established defining equations, and where efficient algorithms and codes have been developed.

In this work, we introduce the Atomistic Global Optimization X (AGOX) framework and python package. AGOX is modular and flexible such that many popular global optimization algorithms can be formulated in the framework and realized in the code. The package builds on the atomistic simulation environment[75] (ASE) and can thus be used with a multitude of electronic structure codes, with a similar focus on effortless scripting as ASE enables. An overview of the framework is presented, and the goals of the code are discussed in detail. We present applications of the code on several systems,

a)Electronic mail: hammer@phys.au.dk

GOFEE

BH   **EA**

RSS
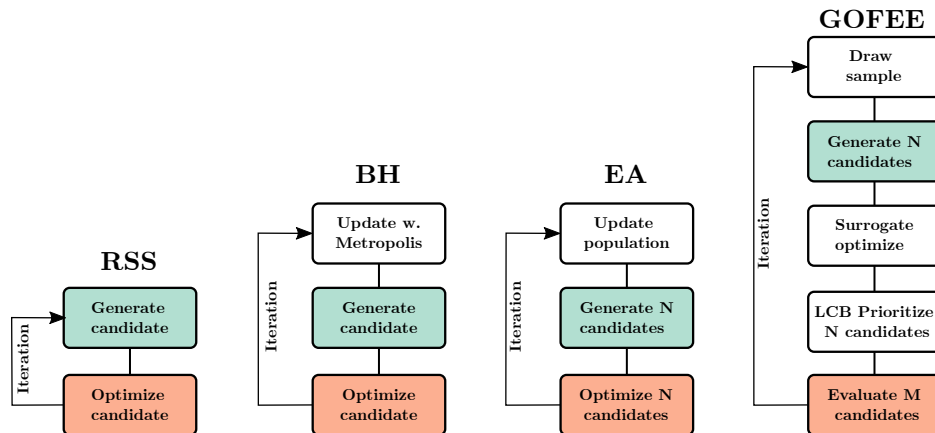
FIG. 1: Overview of several popular global optimization algorithms. Random structure search (RSS) represents the simplest method. In each iteration of RSS, a structural candidate is generated and locally optimized. In basin-hopping (BH), the current position in the search-space is kept track of and updated using the Metropolis criterion. The position is then used by the generation mechanism. In the evolutionary algorithm (EA), a population of candidates is maintained of and serves as input to the generation of a new candidate in each iteration which is then optimized. In GOFEE, a number of candidates are generated and are locally optimized in a computationally inexpensive surrogate potential before deciding on which candidate to evaluate in the true potential using a lower confidence bound acquisition function. The orange boxes will for many problems involve computationally expensive potentials such as DFT.

starting with a cluster on a metal surface described by a cheap potential that is solved using four different global optimization algorithms. A second application is used to highlight the ability of AGOX to surgically make algorithmic changes for a tin-oxide surface system, where basin-hopping and a machine learning enhanced basin-hopping algorithm are compared. The third example is used to discuss parallelization options, where parallel tempering[76] is used to solve a two-dimensional carbon cluster show casing how it is possible to take advantage of computational resources to reduce waiting time for results. The fourth and final example documents considerations taken when solving a computationally demanding problem, in this case a metal-nitride cluster embedded in a graphene sheet where also spin polarization must be taken into account. The AGOX code is freely available on gitlab `https://gitlab.com/agox/agox`.

II. METHOD

A. AGOX Framework

A large number of global optimization methods have been proposed, some of which differ only slightly while others differ significantly, however, all of them involve two essential steps. The first step is the generation of a candidate structure and the second is the evaluation of the generated candidate in the target potential. In Figure 1 examples of global optimization methods having these two steps are given. The first example given is random structure search (RSS), that consists of just

candidate generation and local optimization. The next examples are basin-hopping (BH) and evolutionary algorithms (EA) that both use previous structures as the starting point for the generation, i.e. a perturbation of the atomic positions or as a crossover mutation that combines two or more structures. They therefore need to keep track of which previous structures are used in this way. The final example is the global optimization with first-principles energy expressions (GOFEE) method,[57] in whih the expensive local optimization in the target potential is replaced by local optimization in an on-the-fly trained surrogate potential. Due to the much reduced cost, several candidates may be optimized per iteration and a small number of them may be selected for evaluation in the target potential.

AGOX is a framework that allows all of these algorithms, and more, to be used within a single codebase. This is achieved by defining a number of modules that can be used to build this wide range of optimization algorithms. At present, we have identified the need for two data-type modules and eight action-type modules. The data-type modules enable the handling of the candidates and are as follows:

The ENVIRONMENT module handles the simulation cell, any already present atoms (which we call a template) and the number and species of the atoms the search algorithm should place. This is the fundamental module that defines the properties of the global optimization problem.

The CANDIDATE module manages all the information about the structural candidates, e.g. position of the atoms by inheriting functionality from the ASE Atoms object, and by what means the candidate originated.
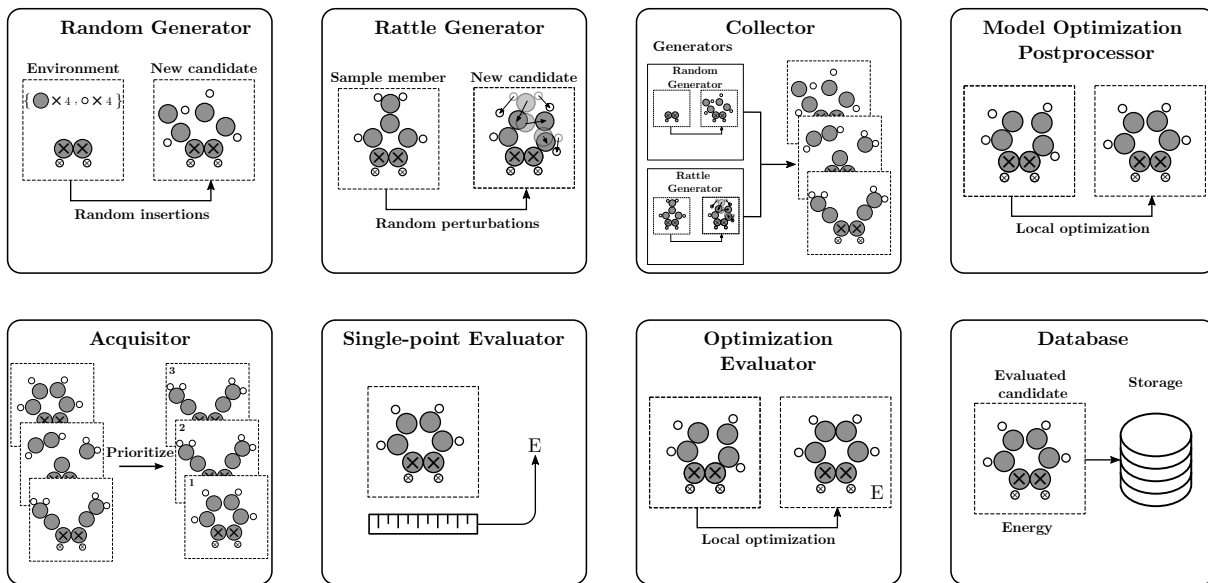
FIG. 2: Pictorial illustration some of the action-type AGOX modules. GENERATORS generate candidate structures, a random generator places atoms at random with the only requirement that bond lengths are within are not too short or too long, whereas a rattle generator perturbs a previously evaluated structure. A COLLECTOR may be used to collect several generated candidates. POSTPROCESSORS may be used to improve generated candidates regardless of which generator they originate from, such as local optimization in a model or moving to the center of a cell. An ACQUISITOR can be used to select the most promising candidate. EVALUATORS calculate key properties of candidates, e.g. the energy and the evaluated structure is stored in a DATABASE.

The action-type modules perform actions based on the structural information in objects from the data-type modules and do in some cases update one or several candidate objects. The eight action-type objects are:

The DATABASE module stores the proposed solutions, that obey the conditions defined by the environment. These may be candidates whose properties have not yet been calculated in the target potential, or structures for which such properties are indeed available. The database represents all the knowledge gathered about the target potential that can be analyzed at the end of the search to determine the global minimum energy structure. Furthermore, several other modules can leverage the information stored in the database during the search, e.g. to build machine learning potentials, to maintain a population, or to extract a sample.

The MODEL module builds machine learning potentials, such as the gaussian process regression model employed by GOFEE, based on the structures stored in the database.

The SAMPLER module provides one or more structures to be used by other modules of the search algorithm to further exploitation of structurally unique areas of search space, or to serve as input in the formation of new candidates causing further exploration of non-visited regions of search space. Depending on the implementation, the module can do so based on all previously studied structures (or even proposed candidates) or it can maintain a population of selected structures, Figure 3 depicts

three different ways that a sampler may function. In basin-hopping, the sampler would use the metropolis acceptance criterion to decide whether or not to update the sample according to the most recently evaluated candidate. In an evolutionary algorithm, the sampler would maintain a population of candidates that are structurally diverse which can be used as parents for subsequent candidates. In general, the sampler can be dependent on the order in which the data is obtained or it can be a function of the gathered data, as is the case for the K-means sampling technique[77] we employ for GOFEE searches in this paper.

The GENERATOR module produces new candidates either by manipulating structures taken from the sampler module or through stochastic process that somehow proposes a set of coordinates, e.g. by placing the atoms randomly in the simulation cell. Generators can be biased in a number of ways that may improve the performance of the search for a set of problems.

The COLLECTOR module manages the generation of new candidates. In general, more than one candidate may be generated at a time and the collector module defines how many candidates are generated using each type of generator, e.g. a preset number of each, a probability for each - or even as a function of the number of iterations.

The POSTPROCESSOR module performs actions on the generated candidates. This could be local optimization of the candidate in a machine learning model potential.
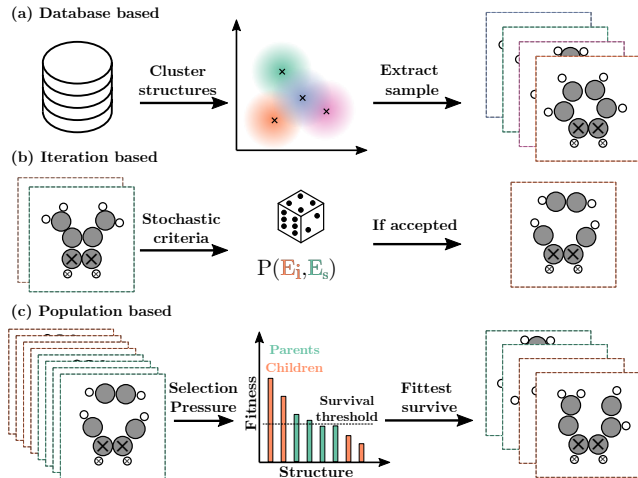
FIG. 3: The starting point of candidate generation can be decided by a $\boxed{\text{SAMPLER}}$. This decision can taken in a number of ways, such as based on the collected data as depicted in (a). It may also depend only on the most recently evaluated structure as depicted in (b). A population-based sampling scheme is depicted in (c). Here, parent and child structures are put under selection pressure where only the fittest structures are allowed to survive to the next generation. The modularity of AGOX makes experimentation using different sampling strategies easy.

The postprocessor may also discard a candidate if it consists of multiple unbonded fragments or if it has some unfavourable atomic arrangements, e.g. an expected too short bond, an unphysical local coordination, or a too high local energy according to a machine learning model.

The $\boxed{\text{ACQUISITOR}}$ module decides which candidates are evaluated in the target potential. This concept is based on Bayesian approaches, such as BOSS or GOFEE,[53,57] but it is implicitly a part of all global optimization algorithms as the choice of which candidates to evaluate in the target potential is central to the global optimization task. Some popular global optimization algorithms, such as BH or RSS, implicitly use an acquisitor that accepts all generated candidates. GOFEE on the other hand leverages Bayesian statistics to intelligently decide which candidate out of a collection of candidates is most likely to further progress the search. So, while the term *acquisitor* is derived from Bayesian methods, it is in fact something all global optimization methods apply.

The $\boxed{\text{EVALUATOR}}$ module evaluates the property of interest for the next candidate. This may be the single candidate produced in a RSS or BH search or the most promising candidate in a GOFEE search. In this work, the total energy in the target potential is the property of interest, but evaluators for other properties can be added such that these properties may be optimized for. Two types of evaluators are used in this work, one that
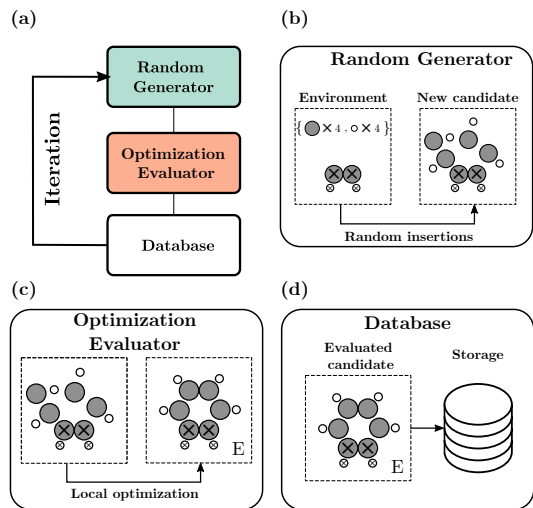
FIG. 4: (a) Flow diagram of a random-structure search algorithm shown in terms of the involved action-type AGOX modules. (b)(c)(d) Illustration of the actions within the modules.

performs a local geometry optimization used with the RSS, BH and EA algorithms and one that just performs a single-point calculation used with GOFEE. Another possibility is to do a limited number, N_s, of relaxation steps in the target potential. In GOFEE it has been suggested to use $N_s = 1$ meaning that a total of two single-point DFT calculations are performed, an approach dubbed "dual-point evaluation".[57]

In Figure 4 we show the modules involved in a random-structure search. Figure 4(a) depicts the flow diagram for the three action-type modules while Figure 4(b)(c)(d) details it further with the pictorial illustrations of the modules.

The framework does not require that the modules are used in any specific order or that all of them are used. This makes the framework very flexible. It is enabled by an observer-pattern, which is a software design technique that will be discussed further in the next section along with the goals of the code.

B. Code

The modules described in section II A are abstractions that we believe are useful when thinking about and describing atomistic global search algorithms. In order to use them in practice they need to be translated into code. It is, however, worth discussing briefly what makes a codebase useful. Our focus has been on three goals

- Ease of development.

- Ease of use.

- Performance (where necessary).

Here, ease of development covers everything from testing new ideas to fully implementing new algorithms. Ease of use enables new users to efficiently utilize the code even though they may not be experts in the field. Finally, any code needs to be performant, however whereas the previous points largely go hand in hand, performance can come at the cost of increased complexity. For many atomistic search problems, the most time-consuming step will be the quantum mechanical calculation of the total energy in the target potential, e.g. density functional theory (DFT). In order to leverage the many efficient electronic structure codes available, AGOX uses the atomistic simulation environment package[75] (ASE) which has Python interfaces to a large collection of codes. Compared to the time of a DFT calculation, the generation of a candidate structure is very fast, even without extremely optimized code. Therefore, for such modules it is more important that the code is easy to understand and fast to develop further. Even though local optimization in a machine learning potential is many orders of magnitude faster than in DFT, the computational time spent in optimizing many candidates may become comparable to that spent in a single-point DFT calculation. Therefore, it is worth some additional complexity to ensure that such optimizations are done efficiently.

In order to ensure both ease of use and ease of development, we take advantage of the objective-oriented programming (OOP) capabilities of the Python language. An abstract base class (ABC) has been implemented for each of the modules of the framework. These are essentially code templates that define the required methods and attributes of an actual specific implementation of any of the modules. The ABC may also define a number of functions that are generally convenient for that particular module, such as checking whether a set of coordinates have chemically valid bond lengths. This improves both the readability of the code by hiding the details behind a method-call when those details are not necessary and the reliability by only having one common implementation for each such method. The OOP design also allows us to leverage inheritance when developing new features in two ways. The first is as mentioned when a new version of one of the modules of the framework inherits from the ABC and the second when an implementation inherits from another specific implementation. Inheritance is depicted in Figure 5.

To make the framework as flexible as possible, we do not wish to impose any restrictions on how the modules are used to design a search algorithm. This means, that it has to be possible to leave out a module, change the order of modules and use multiple versions of the same module. This is accomplished by building an observer-pattern into the core iterative loop.[78] An observer-pattern is a software design technique that entails a subject maintaining a list of its observers that it will notify when changing its state. In AGOX, this state is the iteration counter and observers, which are AGOX action-type modules, will be notified in a pre-specified order in each iteration.
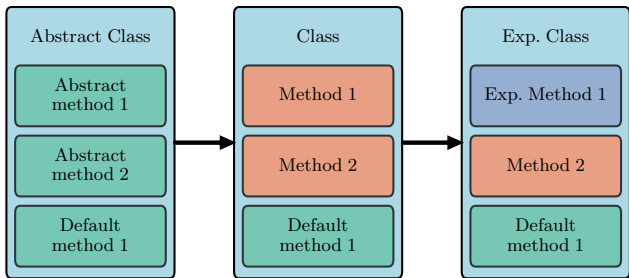
FIG. 5: Illustration of inheritance from an abstract base class shown on the left. The ABC defines two abstract methods and a single default method, a specific version of the class (middle) requires real implementations of the two abstract methods. Experiments with the functionality of this specific version can be performed by inheriting from the it and surgically replacing only the relevant method.

By changing the list of observers one may alter what the program actually does. Importantly, this can be done without altering the code of any of the modules or the core iterative loop. Each module acts as an observer that can read and write to a shared data collection, such that there is no hardcoded order of execution. A valid AGOX program can range from a for-loop that does nothing each iteration to a GOFEE search and beyond.

Examples of such observer-pattern based algorithms are depicted in Figure 6. The RSS method, shown in Figure 6(a), has three observer-type modules attached to the iteration loop. Similarly, the BH method may be implemented with four observer type modules attached to the iteration loop, as shown in Figure 6(b). Since the observer-pattern is also built into the DATABASE module, an alternative implementation of the BH methods can be layed out as shown in Figure 6(c). Here, the SAMPLER module is moved from being an observer on the main iteration loop to being an observer on the DATABASE module. In this implementation, the SAMPLER module is invoked whenever new DFT-level data has been dealt with by the DATABASE module. The observer pattern on the DATABASE module is also exploited in the implementation of the GOFEE method presented in Figure 6(d). Here, it is the update of the MODEL that is invoked whenever the DATABASE module has handled new DFT level data. To allow decoupling of modules, such that e.g. a POSTPROCESSOR does not expect input from a GENERATOR or any other instance of hard coded interdependence, the communication between modules is handled by a shared cache or through the database, as depicted in Figure 7.

A useful way of thinking about an AGOX program is to consider it a set of functions that are executed in an order specified in a script, rather than by the underlying core code and without any predefined relations be-
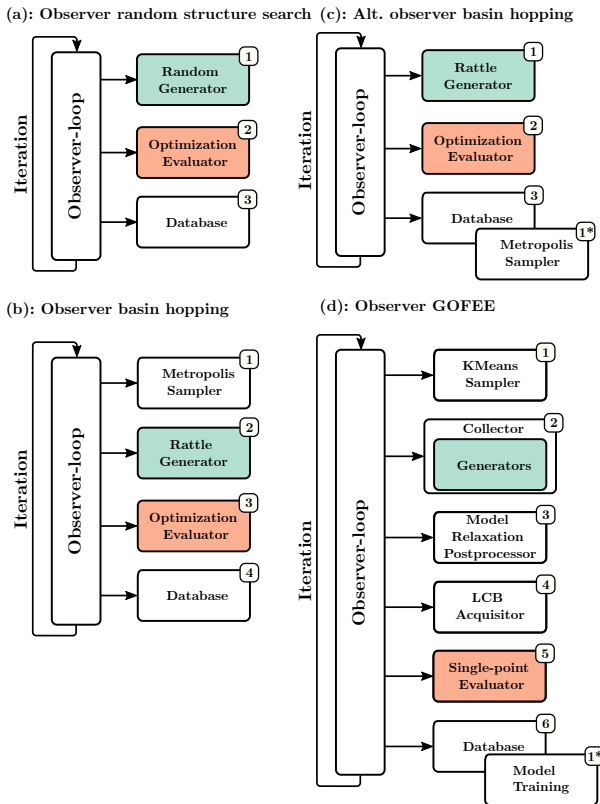
FIG. 6: Several global optimization algorithms programmed in different ways. The observer-pattern loop allows different algorithm to be expressed using the same modules. The numbers note the order of execution, which the observer-pattern takes into account. A module may also be an observer to the database and be notified whenever new data is added. This is depicted for the sampler module of basin-hopping and the model training function in GOFEE.

tween the set of functions. AGOX is designed to work based on definition and assembly of such functions via definition of modules at the scripting level since it provides an easy and logical way of handling algorithms deficient of certain actions. Imagine, by the contrary, that connections between the modules were indeed hardcoded to e.g. match the GOFEE layout presented in Figure 1, then the RSS algorithm could still be formulated having versions of certain modules that would do essentially nothing, e.g. the acquisitor, the sampler and the postprocessors. With the observer-pattern these modules can be left out entirely. Another advantage granted by the observer-pattern is that new modules may be included in the future, again because the order of execution and the communication between modules is not predefined.
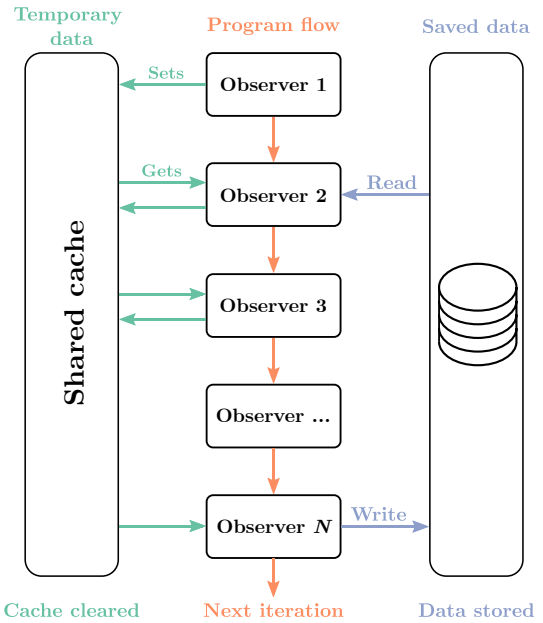
FIG. 7: Depiction of the program flow and data access of an AGOX algorithm. Here, an abstract algorithm is depicted as a series of observers, each of which have the ability to get or set data in the shared cache. Additionally, modules can have access to the database. At the end of an iteration the shared cache is cleared, whereas data saved to the database is saved permanently. Observers may also communicate with each other through connections defined in the AGOX python script, whenever modules depend on other modules to perform their function. For instance, a generator may be given access to the sampler in order to retrieve sample members.

C. Code example: An acquisitor

As an example of the benefits of the described coding scheme, we will take a look at an acquisitor. The basic acquisitor used for GOFEE type searches is the lower confidence bound (LCB) acquisitor, see Section X A for details. The implementation of LCB inherits from the acquisitor ABC, in the way depicted in Figure 5. We can easily experiment with alternative acquisition functions, and depending on the type, it can either inherit from the base-class or a specific implementation, e.g. the LCB acquisitor. As an example, we can imagine we would like to try an acquisition function defined by

$$x_a = \underset{x \in X}{\operatorname{argmin}} \left[E(x) - \kappa \sigma(x)^\rho \right], \tag{1}$$

where X is a set of candidate coordinates, $E(x)$ and $\sigma(x)$ are surrogate energy and uncertainty functions and κ and ρ are chosen parameters. For $\rho = 1$ this reduces to the LCB expression. This can be implemented in very little code by inheriting from the LCB class.

```
1  class PowerLowerConfidenceBoundAcquisitor(
       LowerConfidenceBoundAcquisitor):
2
3  name = 'PowerLowerConfindenceBoundAcquisitor'
4
5  def __init__(self, rho=1, *args, **kwargs):
6      super().__init__(*args, **kwargs)
7      self.rho = rho
8
9  def acquisition_function(self, E, sigma):
10     return E - self.kappa * sigma ** self.rho
11
12 def acquisition_force(self, E, F, sigma,
       sigma_force):
13     return F - self.kappa * self.rho * sigma**(
           self.rho-1) * sigma_force
```

Thus, in less than 15 lines of code, experiments can be made with a different acquisition function without any risk of causing issues with existing code due to the use of inheritance.

D. Success curves

One key metric to judge the performance of any global optimization algorithm is a success curve, which is a statistical property that measures the percentage of independent search runs or searches that are 'successful' against the number of single-point calculations, iterations or timing metrics. In the used terminology, a search refers to the execution of an algorithm typically for a predetermined number of iterations - although other stopping criteria are also possible. A search produces a number of structures, e.g. a random-structure search of 1000 iterations will produce 1000, not necessarily unique, local minimum energy structures. However, given the stochastic nature of most global optimization algorithms there is no guarantee that a search finds the global minimum structure. Whether or not a single search finds the global minimum also tells us very little about the ability of the algorithm to solve the problem, again due to the stochastic nature, a second search may lead to different results. To compare searches done with different algorithms, or the same algorithm with different parameters, we therefore need a statistical measure that averages over several independent searches, which is exactly what a success curve does. Since the underlying physics is typically not only governed by the global minimum energy structure, but by a collection of low-energy structures, we count structures within some small energy of the best structure found among all searches to be successful in this work. For applications where finding a specific structure is considered the success criterion, a graph-based method for identifying that specific structure can be employed, see Sec. X C. With either success criterion, success curves are informative about the performance of the used algorithm. As such, they can be used as a measure of confidence in the found solution, with high success being required in order to be confident in the solution and the ability of the method to solve more difficult problems. The process of obtaining a success curve is illustrated in Figure 8.
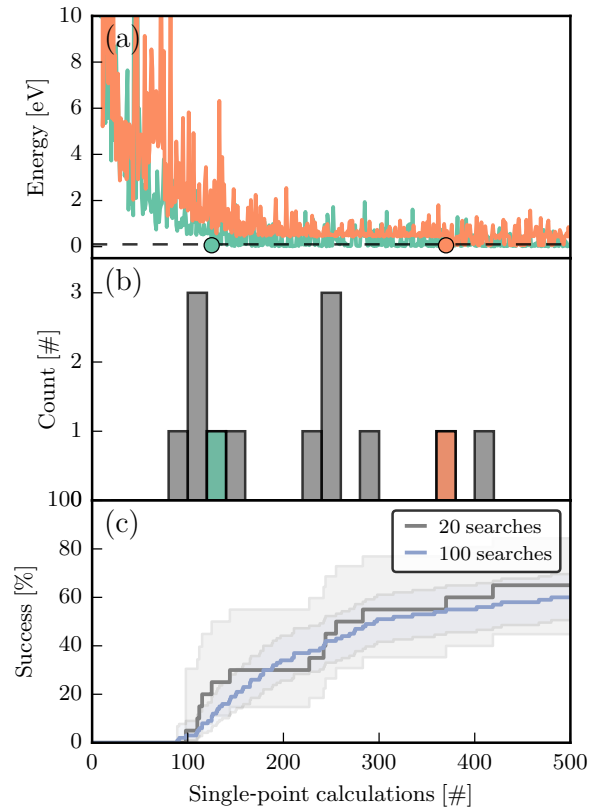
FIG. 8: (a) The energy per single-point calculation for two different searches, the dashed black-line indicates the success criterion. The two-colored dots show when the two searches find a candidate that is considered successful for the first time. In (b) the number of single-point calculations until first success is presented as a histogram, green and orange bars indicate the contributions from the searches in (a). A success curve is obtained by integrating the histogram (with a bin size of 1) and normalizing according to the number of searches, as shown in (c). With more searches the curve becomes smoother and the uncertainty decreases as evidenced in the difference between the gray curve based on 20 searches and the blue based on 100 searches in (c).

III. APPLICATION: GLOBAL OPTIMIZATION ALGORITHMS

As an example of an application of the AGOX framework, we study a system consisting of a platinum cluster on a gold surface described by the simple effective medium theory (EMT) potential[79] as implemented in ASE. This potential is chosen as it works out of the box having installed just ASE and AGOX. We present the results of the application of the AGOX framework using
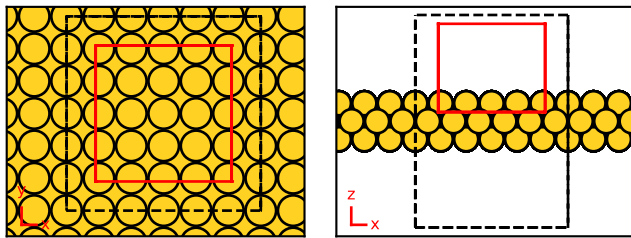
FIG. 9: Gold surface slab used as template for the $Pt_{14}/Au(100)$ search. The computational super cell and confinement cell are depicted in the xy- and xz-planes in black and red, respectively.

four different search algorithms, namely RSS, BH, EA and GOFEE.

In order for an optimization algorithm to be efficient at solving any particular problem it must impose search biases that favour finding the global optimum solution for that particular problem. We distinguish between two kinds of biases. Those that are imposed from the outset and those that are learned by the algorithm. A somewhat trivial example of an imposed bias is the number of atoms, having decided that only 14 Pt atoms are present, the search space is limited to solutions that involve 14 Pt atoms. A less trivial imposed bias, is to constrain the physical space that the algorithm is allowed to use, this is useful as it limits the number of symmetry related solutions, e.g. translations of the cluster along the surface. Learned biases arise from how the algorithm uses the data it gathers during a search. The surrogate potential will impose a learned bias and so will the sampling technique used to decide which previous structures are used to generate new candidates.

In AGOX, the search can be confined to a cell which may differ from the periodic/computational cell used, such that both the generators and the relaxation post-processing will not result in any geometries that have atoms outside of the specified cell. For the $Pt_{14}/Au(100)$ system this is essential to find physical solutions where Pt atoms are only present on one side of the surface slab. This cell is depicted along with the surface slab in Figure 9.

The system-dependent choices, that is the decisions that define the search problem, can be summarized as

- The number of and species of the atoms that are directly involved in the search. (The 14 Pt atoms)

- The template, that is the number and positions of atoms already present in the cell. (The gold surface and cell depicted in Figure 9)

- The confinements, if any. (The confinement cell depicted in red in Figure 9)

The specific choices made here are listed in parenthesis. Each global optimization algorithm has an additional number of options. The action-type observer modules

used in the four methods were set up in the following way and with the following choices for the adjustable parameters:

Random-structure search

$\boxed{\text{GENERATOR}}$: One candidate is generated per iteration using the random generator.

$\boxed{\text{EVALUATOR}}$: The generated candidate is relaxed in the EMT potential until the forces on all Pt atoms are below 0.05 eV/Å, template atoms are fixed, and Pt atoms are not allowed to leave the confinement cell depicted in Figure 9.

Basin-hopping

$\boxed{\text{SAMPLER}}$: A new structure is accepted or rejected using the Metropolis criterion with probability of acceptance given by

$$A = \min\left\{1, \exp\left[\beta(E_{k-1} - E_k)\right]\right\}, \qquad (2)$$

With $\beta = 1/k_BT$ with $k_BT = 1$ eV and E_k is the energy of the structure found in iteration k. If accepted, the structure replaces the previously accepted structure as the starting point of the rattle generator in the next iteration. Skipped in the first iteration.

$\boxed{\text{GENERATOR}}$: Initialized with a random generator, and all subsequent iterations generate one candidate per iteration using a rattle generator applied to the latest structure accepted by the sampler.

$\boxed{\text{EVALUATOR}}$: Same as for RSS.

Evolutionary Algorithm

$\boxed{\text{SAMPLER}}$: A population of 10 structures with diversity enforced using fingerprint feature and parent selection using the algorithm proposed by Vilhelmsen and Hammer.[13]

$\boxed{\text{GENERATORS}}$: Initialized with 10 random generator candidates and with subsequent iterations using 10 candidates generated by rattling structures from the population.

$\boxed{\text{EVALUATOR}}$: Same as RSS for all 10 candidates generated per iteration.

GOFEE

SAMPLER : We use the K-means clustering based sampling method reported by Merte et al.[77] with a total sample size of 10 structures and an energy requirement such that considered structures are within 25 eV of the best structure discovered so far. The method works similarly to the depictions in Figure 3(a) by applying K-means clustering to all evaluated candidates in feature space and selecting structures from each cluster enforcing diversity of the selected structures.

GENERATORS : We use a random generator, a rattle generator and a generation mechanism described by Palecio et. al.[56] that favours perturbing atoms far from the center of geometry of the cluster, which we call center-of-geometry generator. A total of 30 candidates are generated per iteration with 10 candidates from the random generator, 15 from the rattle generator, and five from the center-of-geometry generator.

POSTPROCESSING : All candidates are relaxed in the LCB expression evaluated using the surrogate GPR model until the maximum LCB force ($\kappa = 2$) of non-template atoms is below 0.2 eV/Å. This is done in parallel utilizing all available CPU cores. The relaxation is constrained such that atoms are kept within the confinement cell.

ACQUISITOR : Among the 30 candidates the one with the lowest lower confidence bound ($\kappa = 2$) value is chosen.

EVALUATOR : One single-point calculation is done for the candidate picked by the acquisitor.

MODEL : Details of the GPR model are given in Sections X A and X B.

Results

Four different success curves are presented in Figure 10 that originate from sets of AGOX searches using the four different search algorithms, RSS, BH, EA and GOFEE. The least biased algorithm, random structure search, explores the search space in the least directed way which means it will not become stuck but at an increased computational cost. Basin-hopping, that reuses previous structures in the generation mechanism, is directed towards exploring low-energy regions which results in higher success with fewer single-point calculations. The EA is able to evolve a number of structures, making it more resistant towards getting stuck in a local minimum and enabling slightly better performance compared to the BH in agreement with similar studies.[80] Note that the EA could also use a crossover generation

mechanisms that would involve combining two or more members of its population, but that is not taken advantage of here. Finally, the GOFEE algorithm replaces local optimization in the true potential (EMT) with local optimization in a surrogate GPR model and only does single-point calculations for favorable structures chosen by the LCB acquisition function. This results in orders of magnitude fewer single-point calculations while reaching much higher success. It should be noted that the parameters of each algorithm have not been optimized, as that requires a very large computational effort as a single success curve requires at least tens of searches, likely more to resolve subtle differences for fairly unresponsive parameters. Regardless, the objective here is to showcase that all of the algorithms can be handled within the AGOX framework. Figure 10 does show that the GOFEE algorithm heavily outperforms the other three algorithms in terms of single-point calculations, without the prospect of the others improving enough with optimal parameters to compete with it.

This is not surprising given that GOFEE only performs one single-point calculation per iteration while relying on the surrogate model to get locally optimized structures, which is an algorithmic change rather than due to specific parameter choices. As an EMT potential is used here, it is in fact more computationally demanding to run GOFEE for this problem, as the surrogate potential is not faster to evaluate than the potential, but GOFEE needs to query the potential much fewer times which is the key benefit for problems with a more computationally demanding potential.
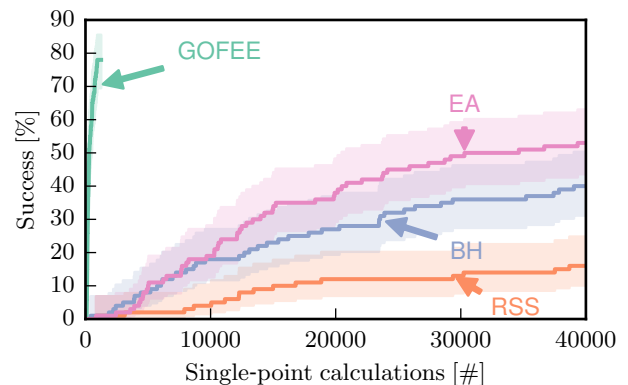
FIG. 10: Success curves for four different global optimization algorithms.

In Figure 11 we report the 15 structures with the lowest energy for the $Pt_{14}/Au(100)$ system. These have been extracted by first obtaining all structures found that are within 0.5 eV of the best structure. Among these, those that have unique graph spectra, according to the method described in Sec. X C are identified and locally optimized, after which the graph spectra are compared once again. It is apparent, that the methods are capable of

finding many distinct low-energy structures and that the graph-based sorting criterion enables the distinction of the different low-energy structures.
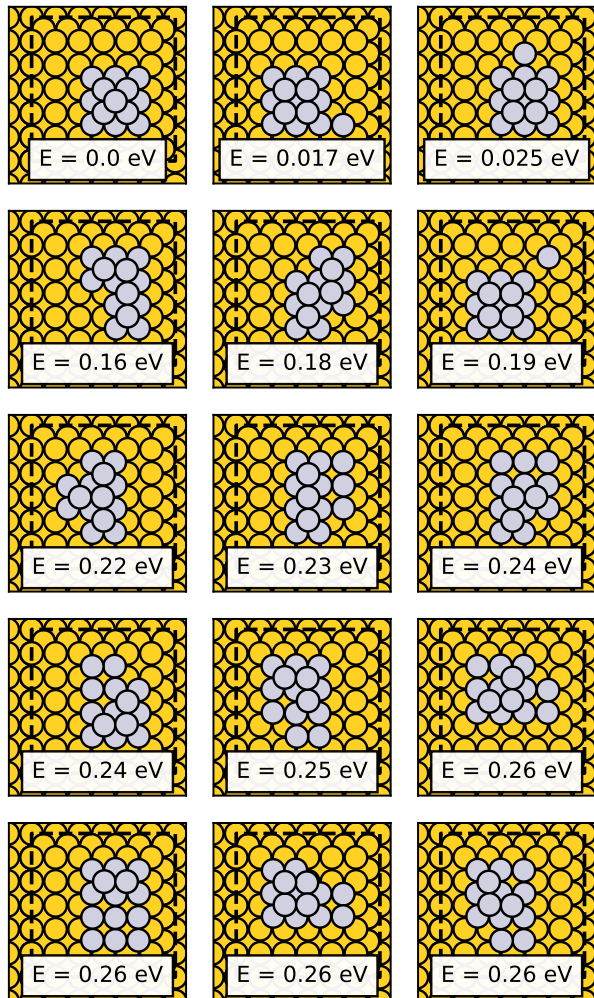
FIG. 11: Low-energy structures of Pt_{14} on Au(100), with the energies relative to the structure with the lowest energy. The structures have been locally optimized after the search such that the maximum force is 0.01 eV/Å.

IV. APPLICATION: MACHINE LEARNING-ENHANCED BASIN-HOPPING

As an example of the ability of AGOX to facilitate the design of global optimization algorithms, we present a comparison of a basin-hopping algorithm and a machine learning-enhanced basin-hopping algorithm. As discussed previously, the most expensive part of a basin-hopping type search is the local optimization, often involving many dozens of electronic structure calculations to obtain the forces on each atom. If some of these calculations can be omitted while retaining
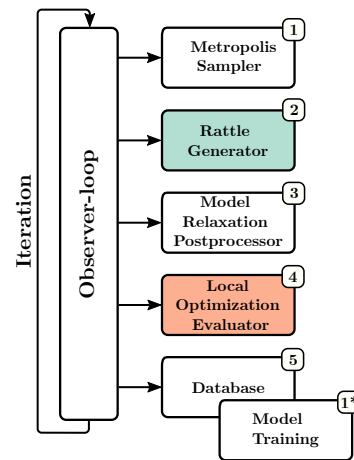
FIG. 12: Basin-hopping search algorithm with a model inserted.

the ability of the algorithm to solve any given problem that would constitute a more computational efficient algorithm.

In AGOX such algorithmic changes can be made easily and surgically requiring only changes to the script and not to the core of the code. These specific changes involve inserting a surrogate model local optimization step between the steps performing candidate generation and candidate optimization as for BH in Figure 1 or in the terminology of AGOX a postprocessor in between the rattle-generator and local optimization evaluator observers of Figure 6(a). The resulting flowchart of the algorithm is shown in Figure 12. The changes compared to a standard basin-hopping search script amount to, defining a model

```
model = ModelGPR.default(environment,
    database)
```

and giving that model to a postprocessor

```
relaxer = RelaxPostprocess(
model=model, start_relax=10,
optimizer=BFGS, optimizer_run_kwargs=
    {'fmax':0.05, 'steps':100},
constraints=environment.get_constraints())
```

and giving those additional modules to the AGOX class

```
agox = AGOX(database, generator, sampler,
    evaluator, relaxer, wrapper)
```

The scripts are available in full at https://gitlab.com/agox/agox_data.

We applied the ML-assisted basin-hopping algorithm to optimizing a rutile $SnO_2(110)$-(4×1) system where 6 Sn and 6 O atoms are arranged on the fixed surface described at the DFT level using an LCAO basis set[81] and the PBE exchange-correlation functional[82] as implemented in GPAW.[83,84] The Γ-point is used for sampling the Brillouin zone and for Sn a 4-valence electron PAW setup is used. The system is shown in Figure 13. The settings of the modules were as follows:
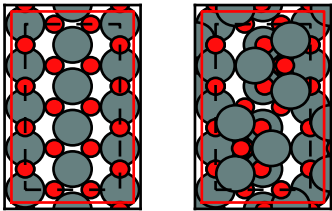
FIG. 13: Left: Template comprising a one-layer rutile $SnO_2(110)$-(4×1) slab. Right: Global minimum energy structure for Sn_6O_6 on $SnO_2(110)$-(4×1). Sn atoms are shown in gray, oxygen atoms are shown in red. The super cell is drawn as a dashed black rectangle. The confinement in the xy-plane is indicated as a red colored rectangle.

ML-enhanced basin-hopping

SAMPLER : Same as for BH in Section III.

GENERATOR : Same as for BH in Section III.

POSTPROCESSOR : Invoking the BFGS optimizer in ASE using the model calculator for up to 100 episodes or until the forces of non-template atoms are below 0.05 eV/Å.

EVALUATOR : Same as for RSS in Section III, except that only a limited number of relaxation steps were done ($N_s = 3$ or $N_s = 10$).

MODEL : Same as for GOFEE in Section III.

In Figure 14, we show success curves for solving this problem with and without locally optimizing in the model prior to doing DFT optimization. For both methods searches, are done with a different maximum allowed number of DFT gradient steps, as that is an important parameter for the ability of standard basin-hopping to solve a problem. In Figure 14(a) we see that using a model much fewer DFT steps are required, which is the same trend observed for the previous system. As the DFT calculation time is the dominating factor a similar trend is observed when plotted against CPU time in Figure 14(b), however the curves using a model are slightly less steep because of the scaling of training and using the model. Finally, in Figure 14(c) the success is plotted against the number of basin-hopping iterations, presenting a remarkable result that even though the model is learning the potential on-the-fly, there is no difference in the number of iterations required to solve the problem. Developments such as the one presented here are enabled by AGOX as algorithms can be altered entirely through a script.
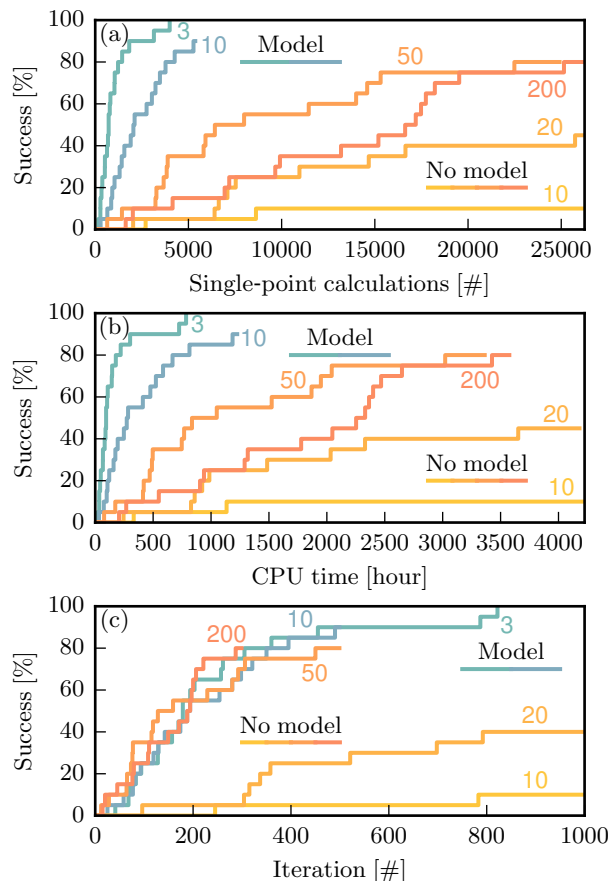
FIG. 14: Success measured against (a) single-point DFT calculations, (b) CPU time and (c) number of basin-hopping iterations. The colored numbers indicate the maximum number of DFT gradient steps allowed in each basin-hopping iteration. The CPU time is derived as 24 times the wall time passed, since the runs were performed on 24 CPU cores in order to speed up the DFT calculations that parallelize well. In (c) the iteration axis has been limited to 1000, the standard basin-hopping searches performing 10 and 20 relaxations steps have run for a total of 2700 and 1400 iterations, respectively.

V. APPLICATION: PARALLEL TEMPERING

An important consideration when building software tools is the ability to take advantage of the ever-increasing number of processor cores in modern computers, be it a desktop computer with a handful of cores or a high-performance computing server with many thousands.

Within a single search run AGOX takes advantage of ASE to run electronic-structure calculations in parallel on the number of processes allotted. Furthermore, in the GOFEE setting, where several candidates are produced per iteration, model relaxations are also parallelized such

that the same number of cores are utilized as for electronic structure calculations.

In general, it is also an advantage to perform several instances of the same search with the same settings in order to have several independent search runs of the algorithm, in order to more thoroughly explore the search-space. Due to the independence of each search, with no communication to any other searches, this is an *embarrassingly* parallel task, and parallelization is as simple as running the same script on several computers - or using a workload manager, such as Slurm commonly available on HPC facilities. This is what is done to make success-curves that require a large number of independent searches as discussed previously, and what we recommend doing when applying AGOX to solve a search problem.

AGOX can, however, also be used to build algorithms that benefit from having several workers. An example of such an algorithm is parallel tempering.[76] In parallel tempering, basin-hopping searches are performed simultaneously at different temperatures. Structures accepted at different temperatures may be swapped to avoid stagnation by promoting exploration at high temperatures and exploitation at low temperatures. In this setting, a search consists of a number of workers using different processors with each worker running a basin-hopping search at one temperature and all workers sharing a single DATABASE .

Structures are swapped between workers with adjacent temperatures every N_t episodes with probability

$$P = \min \left\{ 1, \exp\left(\beta_i - \beta_j\right)(E_i - E_j) \right\} \qquad (3)$$

where $\beta_i = 1/k_B T_i$. Temperatures are chosen according to $k_B T_i = k_B T_0 \cdot (3/2)^i$ where i ranges from zero to the total number of workers N_w minus one in integer steps and $k_B T_0 = 0.05$ eV. Every N_t iterations each worker waits for all other workers of the same search to reach that iteration before reading the database from disk, this is done prior to swapping structures to ensure all workers are synchronized. Compared to a standard basin-hopping search this type of parallel tempering search requires only changing the database module and the sampling module.

Synchronized parallel tempering

SAMPLER : Parallel tempering using the Metropolis criterion of Eq. (2) to decide whether or not to accept a candidate and attempting swaps between candidates at adjacent temperatures every $N_t = 10$ episode according to Eq. (3).

GENERATOR : Same as for BH in Section III.

POSTPROCESSOR : Generated structure is moved to the center of the cell.
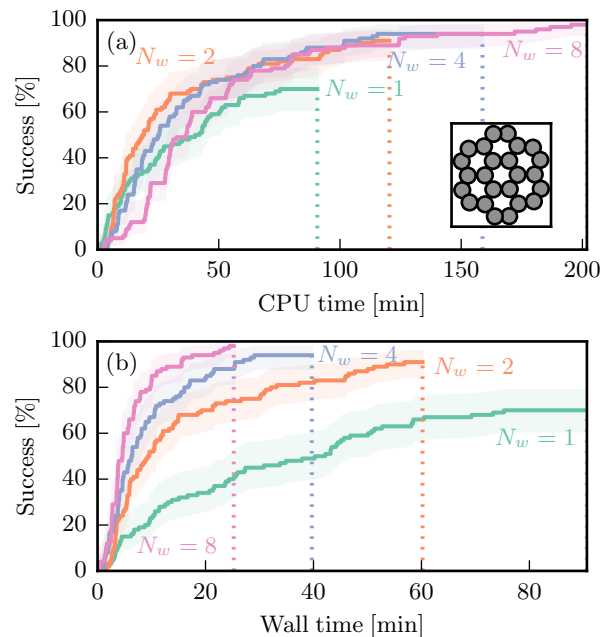
FIG. 15: Success curves for parallel tempering with $N_w = \{1, 2, 4, 8\}$ as a function of (a) CPU time and (b) wall time. In both cases it is the time per independent search. The inset in (a) shows the global minimum structure.

EVALUATOR : Local optimization until forces on all atoms are below 0.2 eV/Å.

DATABASE : Structures are synchronized among workers every N_t iteration.

As an example, we apply this algorithm to a 24-atom carbon cluster constrained to two-dimensions in the search described by the semi-empirical extended tight-binding method (GFN2-xTB).[85,86] To fairly compare searches with different number of workers each search is run for $2000/N_w$ iterations, such that the same number of candidates are generated and locally optimized. Success curves for this system are shown in Figure 15 both as a function of CPU time and wall time in (a) and (b) respectively. The parallel-tempering scheme helps alleviate stagnation, as evidenced by searches with more workers reaching higher success rates for the same amount of CPU time. The overhead introduced by workers having to wait for each other to synchronize the database does make it more expensive in CPU time to do searches with more workers. However, as each worker only has to do a fraction of the work, the wall time, that is the waiting time between starting search runs and achieving results, is decreased significantly.

This example show-cases one example of how AGOX modules may be used to parallelize algorithms. The shared database module can also be used to parallelize

other algorithms implemented in AGOX due to the modularity of the framework. That could for example be random structure search runs, which parallelize trivially, or the model-enhanced basin-hopping example of the previous section, where the model for each search may be updated based on the collected data from all searches.

VI. APPLICATION: EMBEDDED METAL CLUSTER
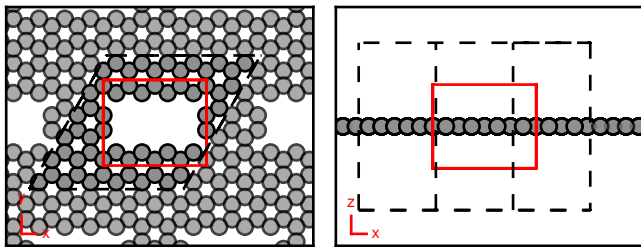
FIG. 16: Template used for $Ru_3N_4C_4$ with the confinement cell shown in red.

Finally, we have applied AGOX to a system that consists of three Ru, four Ni and four carbon atoms that are embedded in a hole in a graphene sheet. This system is inspired by a combined experimental and theoretical study of the properties of such graphene embedded Ru_3N_4 clusters.[87] Here, we only employ the GOFEE algorithm as described in Section III, except the 30 candidates per iteration are generated only with a random generator and a rattle generator, producing 10 and 20 candidates, respectively. The choices of parameters and analysis procedure are not specific to GOFEE and can be used with any global optimization algorithm. Only the three Ru, four Ni and four carbon atoms are allowed to move during the search. To accurately rank the most stable structures, we apply a procedure where all atoms are involved in a local optimization after the global optimization algorithm has finished, this procedure is described in detail below.

The template and confinement used for the search is illustrated in Figure 16, the periodic cell is 16 Å in the z-direction. For this system the search is performed at the DFT level using GPAW[83,84] with a plane wave basis set using an energy cutoff of 300 eV and only a single k-point with the Perdew-Burke-Ernzerhof (PBE) exchange-correlation functional.[82] Further analysis of the found structures is performed with a plane wave energy cutoff of 400 eV and a (3, 3, 1) Monkhorst-Pack k-point grid again with the PBE functional, but now also including the effects of spin polarization. Henceforth, we call the first set of settings the 'rough' settings and the latter set the 'fine' settings.

For studying the physical properties of a system using DFT, it is important that the computational settings are chosen at a sufficient level of precision in order for the

relevant properties to converge. This is typically done by performing convergence checks were each setting is varied until the property of interest is converged within a specified tolerance. For global optimization, the target property is the geometry of low-energy structures, but running the entire search with multiple sets of settings is computationally costly so that cannot generally be done. Furthermore, it is often the case that the geometries converge before their total energies do. It is thus sufficient to perform the search at relatively rough settings with the benefit of decreasing the computational cost. To ensure that correct results are obtained, a number of the most stable solutions can then be investigated using more accurate settings.

The procedure we employ for this $Ru_3N_4C_4$ search problem is

- Run the GOFEE search for a number of independent searches with rough settings.

- Identify the most stable geometries.

- Select those with unique graphs.

- Locally optimize these, without constraining the template atoms, with the rough settings followed by the fine settings.

- Select again those with unique graphs.

- Obtain total energies at higher level of theory, including spin polarization.

In the steps involving local relaxations with either rough or fine settings after the GOFEE search, all atoms are included, i.e. both template atoms and the atoms placed in the search.

In the present work, we have performed 25 independent searches for 1000 iterations, resulting in 25000 structures among which 8685 are within 2 eV of the most stable structure found during the search. These 8685 structures share 120 unique graphs, when using the spectral graph technique described in Section X C. The best structures of each graph is then relaxed in the target potential. Before performing the spin-polarized calculations the graph comparison method was employed again, now with the 120 locally optimized structures, resulting in a final total of 28 unique structures. Spin polarized calculations were performed with the total magnetic moment fixed at 0, 1, 2 and 3 and the initial magnetic moments distributed evenly among the Ru atoms for each of these 28 structures.

The 10 most stable structures found by employing this procedure are depicted in Figure 17. For the search, the most stable structure found is structure two, however after local optimization with the same settings as used for the search, without fixing the graphene sheet, structure three becomes the most stable. Structures four and five
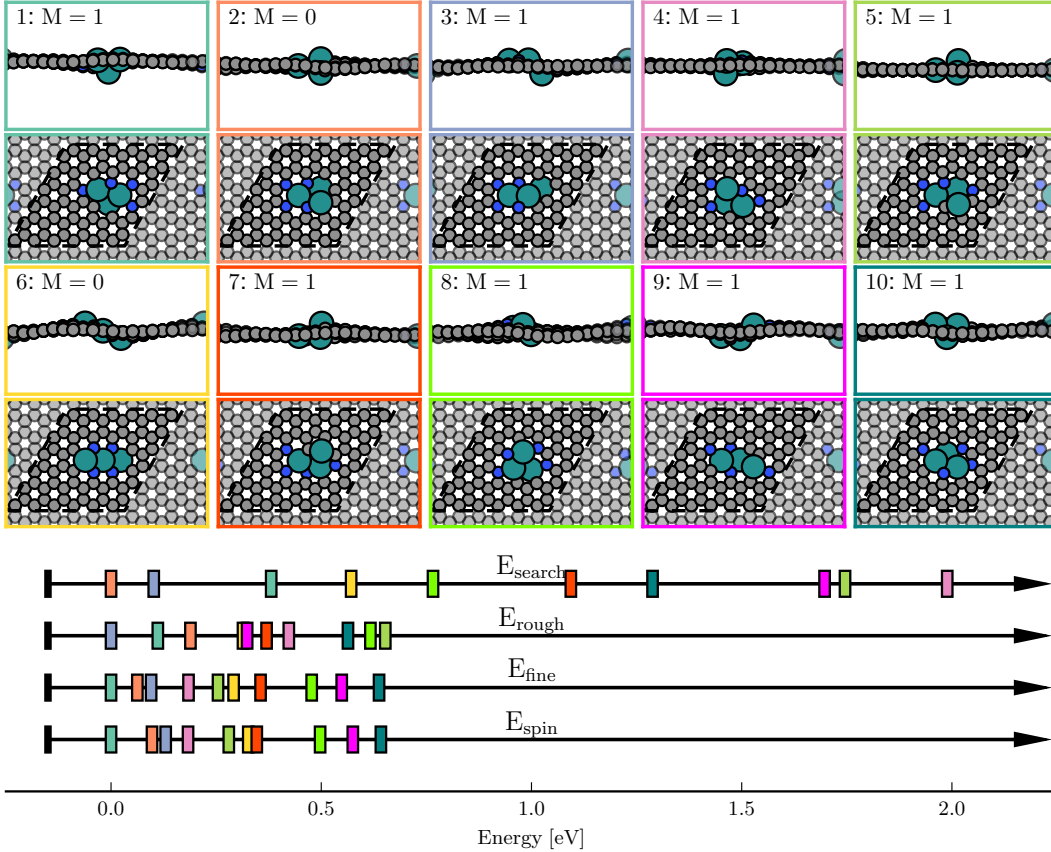
FIG. 17: Most stable structures found for search of Ru_3N_4 in a graphene sheet. The bar plot shows the energy relative to the most stable structure at that step of the procedure. The most stable structure identified by the search is structure two, but at the higher level of accuracy structure one has a lower energy. Note that because structure 0 lowers its energy more by the inclusion of spin than the other structures, the relative energy of the other structures including spin is higher than when spin is not included even if their energy also decrease. The total magnetic moment M that leads to the lowest total energy is reported along with each structure.

both decrease their total energy by over 1 eV as a result of the local optimization, going from being uncompetitive structures to being possible candidates for the global minimum. This can be attributed to local optimization of the graphene sheet being particularly favorable for these two structures. With more accurate DFT settings structure 1 becomes the most stable structure and the inclusion of spin further decreases its energy relative to the other structures. Structure one, two, three and five all show the triangular arrangement of the Ru atoms that is expected from the experimental results presented by Shufang et. al.[87] We note that in their work, a structural model several eV above the ones shown in Figure 17 was proposed. This highlights the need for efficient and easy to use global optimization algorithms, as even with experimental evidence as a guide, guessing the global minimum structure for such complex systems is practically impossible.

This analysis shows that some degree of reordering of the stability hierarchy of structures must be accounted

for when using less accurate settings for the potential employed in the search compared to the final desired level of accuracy. This begs the question of why not performing the search at the desired level of accuracy? An answer to that question is shown in Figure 18 which shows that at least twice the computational time budget would be required to do so. The post analysis procedure of local optimization and spin-polarized calculations is relatively cheap as it is only done for the structures identified by the spectral clustering technique.

VII. CONCLUSION

Global optimization is an essential part of the computational treatment of materials. However, its successful application requires choosing an appropriate algorithm according to the difficulty of the problem and the computational demand of the chosen potential. Furthermore, computational modeling of materials in gen-
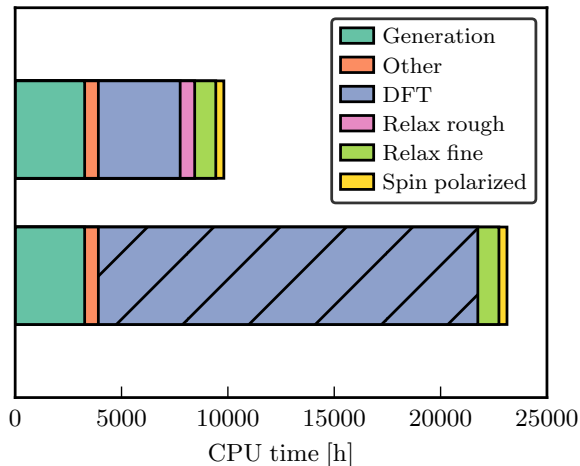
FIG. 18: Breakdown of CPU for the searches performed for $Ru_3N_4C_4$-graphene system. The top bar shows the time for the search performed with fast DFT settings, whereas the bottom bar reports the time if it had been performed with the more accurate DFT settings. A total of $28 \times 4 = 112$ spin-polarized calculations were performed at roughly 3 CPU hours per calculations, compared to the roughly 10 and 40 CPU minutes required for at the low and high unpolarized DFT settings. The hatched area is an estimate based on a single search run with the fine DFT settings.

eral is a rapidly developing field, largely due to the advent of machine learning techniques, it is therefore necessary for software tools to enable these developments. We have introduced the Atomistic Global Optimization X framework and accompanying Python code for the global optimization of atomistic structures that leverage modern programming principles and state of the art machine learning techniques to efficiently solve these tasks. The code is flexible and allows for the rapid development and testing of global optimization algorithms. The application of the package to four examples of global optimization tasks has been documented, one using a simple effective medium theory potential that allows for reproduction of the results with a fairly small computational budget and without installation of additional software. The second example documents how AGOX allows surgically changing algorithms to reduce the computational demand. We also present an application using parallel-tempering that shows how AGOX can take advantage of computational resources through parallelization. Finally, an example show-cases the use of AGOX for a real-world atomistic optimization problem.

VIII. ACKNOWLEDGEMENTS

IX. DATA AVAILABILITY

Version 1.1.0 of the code is publically available at `https://gitlab.com/agox/agox` under a GNU GPLv3 license. Documentation available at `https://agox.gitlab.io/agox`. Data supporting the findings presented in this paper available at `https://gitlab.com/agox/agox_data`.

X. METHODS

A. Gaussian Process Regression

When employing a machined learned model in AGOX we follow Ref. 57 and use a gaussian process regression (GPR) model. With a GPR model, the energy prediction for a structure with feature $\mathbf{x}_*$ is made as:

$$E(\mathbf{x}_*) = K(\mathbf{x}_*, \mathbf{X})[K(\mathbf{X}, \mathbf{X}) + \sigma_n^2\mathbf{I}]^{-1}(\mathbf{E} - \mu(\mathbf{X})) + \mu(\mathbf{x}_*)$$

where μ is the prior, and $\mathbf{E}$ are the energies of training structures that are described by their feature representations $\mathbf{X}$ that are compared by the kernel K for which we use a double Gaussian, as in Bisbo et. al.,[57] where an element is calculated as

$$K(\mathbf{x}, \mathbf{x}_*) = \theta_0\left[(1 - \beta)\exp\left(-\frac{(\mathbf{x} - \mathbf{x}_*)^2}{2l_1^2}\right) + \beta\exp\left(-\frac{(\mathbf{x} - \mathbf{x}_*)^2}{2l_2^2}\right)\right]$$

where the length-scales l_1 and l_2 are chosen such that $l_1 > l_2$ with $\beta = 0.01$. The GPR model also allows the calculation of the model uncertainty for a query structure

$$\sigma(x_*) = K(\mathbf{x}_*, \mathbf{x}_*) - K(\mathbf{X}, \mathbf{x}_*)^T[K(\mathbf{X}, \mathbf{X}) + \sigma_n^2 I]^{-1}K(\mathbf{X}, \mathbf{x}_*),$$

with σ_n being a noise parameter.

Since the GPR model can estimate the uncertainty, it allows for the use of the lower-confidence-bound (LCB) acquisition function. This is done in GOFEE where candidates are relaxed in the LCB and where the next structure to be evaluated in the target potential is chosen according to

$$x_a = \underset{x \in X}{\operatorname{argmin}}\left[E(x) - \kappa\sigma(x)\right] \quad (4)$$

where X is a set of candidate coordinates and κ is a parameter decided upon prior to starting the search. This procedure is depicted in 19, here three candidate coordinates are generated and locally optimized in the LCB expression with the most promising one, that is the one with the lowest LCB value, picked for evaluation.
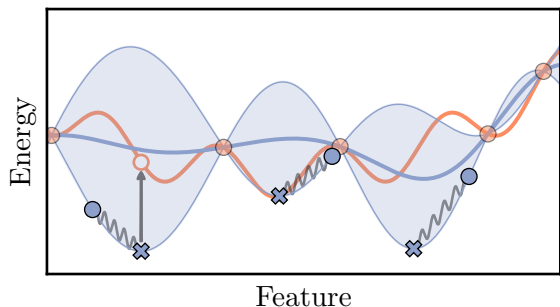
FIG. 19: Example of GPR model and LCB sampling. Orange is the real function from which the orange training points have been gathered, this leads to the blue GPR model where the shaded area represents the uncertainty of the model. By sampling a number of points and relaxing in the LCB surface the next point to evaluate and add to training data may be chosen

B. Fingerprint feature

The representation we employ for the GPR model is the Oganov-Valle fingerprint feature,[88] where the radial components between species A and B are given by

$$
F_{AB}(R) \propto \begin{cases} \sum_{ij} \dfrac{1}{R_{ij}^2} \exp\left(-\dfrac{(R - R_{ij})^2}{2\sigma^2}\right) & , R < R_R, \\ 0 & , R \geq R_R, \end{cases}
$$
(5)

where R_R (6 Å) is a hard cut-off and σ (0.2 Å) is a smearing parameter. A feature vector is constructed by sampling the feature at intervals of Δ (0.2 Å), for multiple species the vectors can are appended together. We also employ angular components, given by

$$
F_{ABC}(\theta) \propto \sum_{ijk} f_c(r_{ij}) f_c(r_{ik}) \exp\left(-\dfrac{(\theta - \theta_{ijk})^2}{2l_\sigma^2}\right)
$$
(6)

where l_σ (0.2 rad) is a smearing parameter and $f_c(r)$ is a cut-off function that ensures that the feature smoothly goes to zero at R_θ (4 Å) as controlled by the parameter γ (2), in particular it is

$$
f_c(r) = 1 + \gamma(\frac{r}{R_\theta})^{\gamma+1} - (\gamma+1)(\frac{r}{R_\theta})^\gamma.
$$
(7)

The values given in parenthesis next to each parameter is the value used in this work.

C. Spectral clustering of atomistic structures

Graphs are a natural way of describing atomistic structures, which ball-stick depictions of molecules illustrates clearly. For our purposes graphs are particularly useful in order to analyse the vast amount of data generated

by search algorithms, in order to filter out the unique structures found. We do this by building the adjacency matrix of each structure

$$
A_{ij} = \begin{cases} 0 & \text{if } i = j \\ 1 & \text{if } D_{ij} < 1.3\ d_{cov}(t_i, t_j) \\ 0 & \text{else} \end{cases}
$$
(8)

with t_i being the atomic number of atom i and where D_{ij} is the distance between atoms i and j, and $d_{cov}(t_i, t_j)$ is the sum of covalent radii for atoms of type t_i and t_j. From this a Laplacian matrix may be constructed as

$$
L_{ij} = (\sum_j A_{ij})\delta_{ij} - A_{ij}
$$
(9)

where δ_{ij} is the Kronecker delta. Finally the eigenvalues of the Laplacian $\lambda = \lambda_1, \lambda_2, .., \lambda_n$ may be computed and two structures may be compared by checking that their eigenvalue spectra are equal. Because this procedure is based on the adjacency matrix small variations in bonds lengths do not change the eigenvalues (unless that change causes a bond to break according to Eq. (8)), which is a helpful property when using this feature to find unique structures. While the eigenspectrum of distinct graphs can be equal, this is unlikely to be the case in practice.[89,90] We use this feature to find distinct structures by grouping together all those structures that have equal eigen spectra. Whereas with a more usual continuous atomistic feature, such as the fingerprint feature used for the GPR model, a distance threshold parameter must be chosen. The fingerprint feature describes minute changes in the structure that do not correspond to configurational differences, whereas the graph eigen spectrum for structures with variations in bond lengths is equivalent and therefore a distance threshold is not necessary.

XI. REFERENCES

[1] J. Greeley, T. F. Jaramillo, J. Bonde, I. Chorkendorff, and J. K. Nørskov, Nat. Mater. **5**, 909 (2006).
[2] C. J. Pickard and R. J. Needs, Phys. Rev. Lett. **97**, 045504 (2006).
[3] Z. A. Piazza, H.-S. Hu, W.-L. Li, Y.-F. Zhao, J. Li, and L.-S. Wang, Nat. Commun. **5**, 3113 (2014).
[4] A. Jain, Y. Shin, and K. A. Persson, Nat. Rev Mater. **1**, 15004 (2016).
[5] A. R. Oganov, C. J. Pickard, Q. Zhu, and R. J. Needs, Nat. Rev. Mater. **4**, 331 (2019).
[6] S. Kirkpatrick, C. D. Gelatt, and C. D. Vecchi, Science **220**, 671 (1983).
[7] D. J. Wales and J. P. K. Doye, J. Chem. Phys. A **101**, 5111 (1997).
[8] S. Goedecker, J. Chem. Phys **120**, 9911 (2004).
[9] D. M. Deaven and K. M. Ho, Phys. Rev. Lett. **75**, 288 (1995).
[10] R. L. Johnston, Dalton T. **22**, 4193 (2003).
[11] A. R. Oganov and C. W. Glass, J. Chem. Phys. **124**, 244704 (2006).
[12] S. Q. Wu, M. Ji, C. Z. Wang, M. C. Nguyen, X. Zhao, K. Umemoto, R. M. Wentzcovitch, and K. M. Ho, J. Phys. Condens. Mat. **26**, 035402 (2013).

[13] L. B. Vilhelmsen and B. Hammer, J. Chem. Phys. **141**, 044711 (2014).

[14] J. Roberts, J. R. S. Bursten, and C. Risko, Chem. Mater. **33**, 6589 (2021).

[15] C. J. Pickard and R. J. Needs, J. Phys. Condens. Matter **23**, 053201 (2011).

[16] Y. Wang, J. Lv, L. Zhu, and Y. Ma, Phys. Rev. B **82**, 094116 (2010).

[17] J. Lv, Y. Wang, L. Zhu, and Y. Ma, J. Chem. Phys **137**, 084104 (2012).

[18] J. Behler and M. Parrinello, Phys. Rev. Lett. **98**, 146401 (2007).

[19] A. P. Bartók, M. C. Payne, R. Kondor, and G. Csányi, Phys. Rev. Lett. **104**, 136403 (2010).

[20] J. Behler, J. Chem. Phys. **134**, 074106 (2011).

[21] M. Rupp, A. Tkatchenko, K.-R. Müller, and O. A. von Lilienfeld, Phys. Rev. Lett. **108**, 058301 (2012).

[22] A. P. Bartók, R. Kondor, and G. Csányi, Phys. Rev. B **87**, 184115 (2013).

[23] K. Hansen, F. Biegler, R. Ramakrishnan, W. Pronobis, O. A. von Lilienfeld, K.-R. Müller, and A. Tkatchenko, J. Phys. Chem **6**, 2326 (2015).

[24] F. A. Faber, A. S. Christensen, B. Huang, and O. A. von Lilienfeld, J. Chem. Phys. **148**, 241717 (2018).

[25] J. S. Smith, O. Isayev, and A. E. Roitberg, Chem. Sci. **8**, 3192 (2017).

[26] V. L. Deringer and G. Csányi, Phys. Rev. B **95**, 094203 (2017).

[27] K. T. Schütt, H. E. Sauceda, P.-J. Kindermans, A. Tkatchenko, and K.-R. Müller, J. Chem. Phys. **148**, 241722 (2018).

[28] N. Lubbers, J. S. Smith, and K. Barros, J. Chem. Phys. **148**, 241715 (2018).

[29] V. L. Deringer, N. Bernstein, A. P. Bartók, M. J. Cliffe, R. N. Kerber, L. E. Marbella, C. P. Grey, S. R. Elliott, and G. Csányi, J. Phys. Chem. Lett. **9**, 2879 (2018).

[30] L. Li, H. Li, I. D. Seymour, L. Koziol, and G. Henkelman, J. Chem. Phys **152**, 224102 (2020).

[31] V. Zaverkin, D. Holzmüller, I. Steinwart, and J. Kästner, J. Chem. Theory Comput **17**, 6658 (2021).

[32] J. Timmermann, Y. Lee, C. G. Staacke, J. T. Margraf, C. Scheurer, and K. Reuter, J. Chem. Phys **155**, 244107 (2021).

[33] J. Xu, X.-M. Cao, and P. Hu, J. Chem. Theory Comput **17**, 4465 (2021).

[34] Z. Li, J. R. Kermode, and A. De Vita, Phys. Rev. Lett. **114**, 096405 (2015).

[35] M. Gastegger, J. Behler, and P. Marquetand, Chem. Sci. **8**, 6924 (2017).

[36] V. L. Deringer, M. A. Caro, R. Jana, A. Aarva, S. R. Elliott, T. Laurila, G. Csányi, and L. Pastewka, Chem. Mater. **30**, 7438 (2018).

[37] V. L. Deringer, N. Bernstein, A. P. Bartók, M. J. Cliffe, R. N. Kerber, L. E. Marbella, C. P. Grey, S. R. Elliott, and G. Csányi, J. Phys. Chem. Lett. **9**, 2879 (2018).

[38] R. Jinnouchi, J. Lahnsteiner, F. Karsai, G. Kresse, and M. Bokdam, Phys. Rev. Lett. **122**, 225701 (2019).

[39] F. Noé, A. Tkatchenko, K.-R. Müller, and C. Clementi, Annu. Rev. Phys. Chem. **71**, 361 (2020).

[40] J. S. Lim, J. Vandermause, M. A. van Spronsen, A. Musaelian, Y. Xie, L. Sun, C. R. O'Connor, T. Egle, N. Molinari, J. Florian, K. Duanmu, R. J. Madix, P. Sautet, C. M. Friend, and B. Kozinsky, J. Am. Chem. Soc. **142**, 15907 (2020).

[41] L. Böselt, M. Thürlemann, and S. Riniker, J. Chem. Theory Comput **17**, 2641 (2021).

[42] R. Ouyang, Y. Xie, and D. Jiang, Nanoscale **7**, 14817 (2015).

[43] T. K. Patra, V. Meenakshiundaram, J.-H. Hung, and D. S. Simmons, ACS Comb. Sci. **19**, 96 (2017).

[44] H. Zhai and A. Alexandrova, J. Chem. Theory Comput. **12**, 6213 (2016).

[45] S. Jindal, S. Chiriki, and S. S. Bulusu, J. Chem. Phys. **146**, 204301 (2017).

[46] V. L. Deringer, D. M. Proserpio, G. Csányi, and C. J. Pickard, Faraday Discuss. **211**, 45 (2018).

[47] A. Denzel and J. Kästner, J. Chem. Phys. **148**, 094114 (2018).

[48] E. G. del Río, J. J. Mortensen, and K. W. Jacobsen, Phys. Rev. B. **100**, 104103 (2019).

[49] G. Schmitz and O. Christiansen, J. Chem. Phys. **148**, 241704 (2018).

[50] Q. Tong, L. Xue, J. Lv, Y. Wang, and Y. Ma, Faraday Discuss. **211**, 31 (2018).

[51] E. L. Kolsbjerg, A. A. Peterson, and B. Hammer, Phys. Rev. B. **97**, 195424 (2018).

[52] T. L. Jacobsen, M. S. Jørgensen, and B. Hammer, Phys. Rev. Lett. **120**, 026102 (2018).

[53] M. Todorović, M. U. Gutmann, J. Corander, and P. Rinke, Npj Comput. Mater. **5**, 35 (2019).

[54] P. C. Jennings, S. Lysgaard, J. S. Hummelshøj, T. Vegge, and T. Bligaard, Npj Comput. Mater. **5**, 46 (2019).

[55] E. V. Podryabinkin, E. V. Tikhonov, A. V. Shapeev, and A. R. Oganov, Phys. Rev. B **99**, 064114 (2019).

[56] M. L. Palecio and J. Behler, J. Chem. Phys **153**, 054704 (2020).

[57] M. K. Bisbo and B. Hammer, Phys. Rev. Lett. **124**, 086102 (2020).

[58] S. Kaappa, E. G. del Río, and K. W. Jacobsen, Phys. Rev. B **103**, 174114 (2021).

[59] M. Arrigoni and G. K. H. Madsen, npj Computational Materials **7**, 71 (2021).

[60] Y. Yang, O. A. Jiménez-Negrón, and J. R. Kitchin, J. Chem. Phys **154**, 234704 (2021).

[61] V. Sumaria and P. Sautet, Chem. Sci. **12**, 15543 (2021).

[62] E. Musa, F. Doherty, and B. R. Goldsmith, Curr. Opin. Chem. Eng. **35**, 100771 (2022).

[63] M. S. Jørgensen, M. N. Groves, and B. Hammer, J. Chem **13**, 1486 (2017).

[64] S. A. Meldgaard, E. L. Kolsbjerg, and B. Hammer, J. Chem. Phys **149**, 134104 (2018).

[65] M. S. Jørgensen, U. F. Larsen, K. W. Jacobsen, and B. Hammer, J. Chem. Phys. A **122**, 1504 (2018).

[66] K. H. Sørensen, M. S. Jørgensen, A. Bruix, and B. Hammer, J. Chem. Phys. **148**, 241734 (2018).

[67] M. S. Jørgensen, H. L. Mortensen, S. A. Meldgaard, E. L. Kolsbjerg, T. L. Jacobsen, K. H. Sørensen, and B. Hammer, J. Chem. Phys **151**, 054111 (2019).

[68] C. J. Pickard, Phys. Rev. B **99**, 054102 (2019).

[69] S. Chiriki, M.-P. Christiansen, and B. Hammer, Phys. Rev B **100**, 235436 (2019).

[70] Z. Zhou, S. Kearnes, L. Li, R. N. Zare, and P. Riley, Sci. Rep **9**, 10752 (2019).

[71] S. A. Meldgaard, H. L. Mortensen, M. S. Jørgensen, and M. S. Hammer, J. Condens. Matter Phys. **32**, 404005 (2020).

[72] G. N. C. Simm, R. Pinsler, and J. M. Hernández-Lobato, "Reinforcement Learning for Molecular Design Guided by Quantum Mechanics," (2020), in International Conference on Machine Learning, 2020, arXiv:2002.07717.

[73] G. N. C. Simm, R. Pinsler, G. Csányi, and J. M. Hernández-Lobato, "Symmetry-Aware Actor-Critic for 3D Molecular Design," (2020), in International Conference on Learning Representations 2021, arXiv:2011.12747.

[74] S. Kaappa, C. Larsen, and K. W. Jacobsen, Phys. Rev. Lett. **127**, 166001 (2021).

[75] A. H. Larsen, J. J. Mortensen, J. Blomqvist, I. E. Castelli, R. Christensen, M. Dułak, J. Friis, M. N. Groves, B. Hammer, C. Hargus, E. D. Hermes, P. C. Jennings, P. B. Jensen, J. Kermode, J. R. Kitchin, E. L. Kolsbjerg, J. Kubal, K. Kaasbjerg, S. Lysgaard, J. B. Maronsson, T. Maxson, T. Olsen, L. Pastewka, A. Peterson, C. Rostgaard, J. Schiøtz, O. Schütt, M. Strange, K. S. Thygesen, T. Vegge, L. Vilhelmsen, M. Walter, Z. Zeng, and K. W. Jacobsen, J. Condens. Matter Phys. **29**, 273002 (2017).

[76] D. A. Kofke, J. Chem. Phys. **117**, 6911 (2002).

[77] L. R. Merte, M. K. Bisbo, I. Sokolović, M. Setvín, B. Hagman, M. Shipilin, M. Schmid, U. Diebold, E. Lundgren, and B. Hammer, Angew. Chem., Int. Ed. Engl. **61**, e202204244 (2022).

[78]E. Gamma, R. Helm, J. Vlissides, and R. Johnson, *Design Patterns: Elements of Reusable Object-Oriented Software* (Addison-Wesley Professional, 1994).

[79]K. W. Jacobsen, J. K. Norskov, and M. J. Puska, Phys. Rev. B **35**, 7423 (1987).

[80]M. N. Bauer, M. I. J. Probert, and C. Panosetti, J. Phys. Chem. A **126**, 3043 (2022).

[81]A. H. Larsen, M. Vanin, J. J. Mortensen, K. S. Thygesen, and K. W. Jacobsen, Phys. Rev. B **80**, 195112 (2009).

[82]J. P. Perdew, K. Burke, and M. Ernzerhof, Phys. Rev. Lett. **77**, 3865 (1996).

[83]J. J. Mortensen, L. B. Hansen, and K. W. Jacobsen, Phys. Rev. B **71**, 035109 (2005).

[84]J. J. Enkovaara, C. Rostgaard, J. J. Mortensen, and et al., J. Phys. Condens. Matter **22**, 253202 (2010).

[85]C. Bannwarth, S. Ehlert, and S. Grimme, Journal of Chemical Theory and Computation **15**, 1652 (2019).

[86]C. Bannwarth, E. Caldeweyher, S. Ehlert, A. Hansen, P. Pracht, J. Seibert, S. Spicher, and S. Grimme, WIREs Computational Molecular Science **11**, e1493 (2021).

[87]S. Ji, Y. Chen, Q. Fu, Y. Chen, J. Dong, W. Chen, Z. Li, Y. Wang, L. Gu, W. He, C. Chen, Q. Peng, Y. Huang, X. Duan, D. Wang, C. Draxl, and Y. Li, J. Am. Chem. Soc **139**, 9795 (2017).

[88]M. Valle and A. R. Oganov, Acta Crystallogr. A. **66**, 507 (2010).

[89]R. C. Wilson and P. Zhu, Pattern Recognit **41**, 2833 (2008).

[90]P. Wills and F. G. Meyer, PLOS ONE **15**, 1 (2020).